

Feb 26th, 11:00 AM

# A Statistical Approach for Commercial Space Vehicle Integration into the National Airspace System

Christopher Hays
*Embry-Riddle Aeronautical University*, haysc3@my.erau.edu

Daniel Chu
*Embry-Riddle Aeronautical University*, chud1@my.erau.edu

Pedro Llanos
*Embry-Riddle Aeronautical University - Daytona Beach*, llanosp@erau.edu

# A Statistical Approach for Commercial Space Vehicle Integration into the National Airspace System

Christopher W. Hays* and Daniel E. Chu.†
*Embry-Riddle Aeronautical University, Daytona Beach, FL., 32114*

Pedro J. Llanos‡
*Embry-Riddle Aeronautical University, Daytona Beach, FL., 32114*

**This paper explores commercial space vehicle (CSV) suborbital flight trajectories in the temporal and spatial domains for CSV integration into the National Airspace System. The research data was collected via the Suborbital Space Flight Simulator (SSFS) housed in the College of Aviation at Embry-Riddle Aeronautical University - Daytona Beach campus, and analyzed using an original MATLAB data analytics tool. This study primarily focuses on statistical trends observed in previously simulated flights supported by three Project PoSSUM (Polar Suborbital Science in the Upper Mesosphere) campaigns comprised of 34 flights and 19 control flights, and to identify relevant milestones in the CSV flight path. The correlations found in these flight milestones are key for the development of a predictive model for flight and ground safety operators, and reduce the necessity for extensively restricted flight hazard areas. In this paper, the PoSSUM and Control flights are compared to evaluate the deviation caused by different thrust operations conducted by the Scientist Astronaut Candidates (SACs) to enhance scientific data collection in the mesosphere. Preliminary results show the adjustments made by the PoSSUM flights have little affect in the domain with a mean difference of 10.4 seconds in time-of-flight (ToF) outside of the NAS, and a noticeable affect in the spatial domain with a mean difference of 9.3 km in the descent threshold range.**

## Nomenclature

| | | |
|---|---|---|
| ATC | = | Air Traffic Control |
| CSV | = | Commercial Space Vehicle |
| ELV | = | Expendable Launch Vehicle |
| FAA | = | Federal Aviation Administration |
| NAS | = | National Airspace System |
| TFR | = | Temporary Flight Restrictions |
| SS2 | = | SpaceShipTwo |
| STC | = | Space Transition Corridor |
| STM | = | Space Traffic Management |
| STS | = | Space Transportation System |
| SUA | = | Special Use Airspace |
| ToF | = | Time of Flight |

## I. Introduction

SPACE launch safety is of primary concern, particularly for any aircraft within the vicinity of a launch. For mitigation of collision, the Federal Aviation Administration (FAA) has implemented a set of criteria for acceptable risk level that establish no-fly zones for any nonessential aircraft. The incorporation of the Temporary Flight Restrictions (TFRs)

*Undergraduate Student, Aerospace Engineering Department, AIAA Student Member.
†Undergraduate Student, Aerospace Engineering Department.
‡Assistant Professor in Spaceflight Operations, Applied Aviation Sciences, Embry-Riddle Aeronautical University, 600 S. Clyde Morris Blvd., Daytona Beach, FL, 32114, AIAA Member

and Special Use Airspaces (SUA) that are both temporally and spatially stringent poses a significant threat to current ATC operations with the projected increase in commercial space traffic traversing the National Airspace System (NAS) [1]. As the frequency of commercial space launches increase, it will become more strenuous on the air traffic industry to maintain nominal operations with TFRs and SUAs consuming the airspace. Currently, if TFRs and SUAs remain the go-to no-fly zones, re-routing flights could cost the airlines up to $\$200,000$ per launch in increased fuel consumption and $2,250$ minutes per launch [2] in cumulative flight delays by the year 2027 .

In an attempt to reduce the effects of temporally and spatially stringent no-fly zones, alternative methods are currently being explored; space transition corridors (STCs) and compact envelopes are tailored restricted airspaces that are temporally and spatially dynamic to mitigate any adverse consequences the increased commercial space flights will have on current NAS operations. Ultimately the implementation of these dynamic STCs will be dependent on the vehicular model used as each vehicle may fall under different return trajectory classifications [3].

- Ballistic - typical return classification of expendable launch vehicles (ELVs) - unpowered and unguided. Vehicle experience free-fall characteristics and less susceptible to atmospheric drift i.e. Space Transportation System (STS) external fuel tank.
- Parachute - commonly used method for return capsule to reduce impact damage - unpowered and unguided. Vehicle highly susceptible to atmospheric drift i.e. manned crew capsules.
- Unpowered glide - vehicle undergoes unpowered flight during reentry - unpowered and guided i.e. Virgin Galactic's SS2, and XCOR Lynx.
- Powered Reentry - similar profile to glide flights without glide limitations - powered and guided. Vehicle may experience free-fall but undergoes powered descent and landing - Falcon 9 first stage.

Depending on the mission profile, differing STCs and compact envelopes may be implemented. For unguided trajectories (ballistic and parachute) the flight paths may be most accurately redicted using high fidelity computational models. These trajectories are mostly unaffected by human intervention, are semi-rigid in flight path, and are highly susceptible to atmospheric conditions; for these reasons, current spatially stringent TFRs and SUAs have been adequate in preserving and protecting the NAS.

With the rise of guided reentry vehicles, the use of TFRs and SUAs is no longer adequate as these flights are not only susceptible to atmospheric conditions, but are also susceptible to pilot intervention. The introduction of a human pilot greatly increases the maneuverability and consequently the variability of nominal flights. Such maneuverability allows for easier integration of guided CSVs without segregation of a larger section of the airspace. Rather, these flights may operate under STCs and compact envelopes during ascent and descent under the NAS ceiling (18,288 m.). This method of operations will allow for satisfactory protection as these guided space vehicles operate within the NAS.

## II. Data Collection and Flight Simulation

Research concerning the implementation of suborbital spaceflight transition corridors is conducted to determine mean points of exit (ascent thresholds) and entry (descent thresholds) of the NAS. The deviations calculated from the experimental data is used to produce ascent and descent zones - warning areas or possible restricted areas that can be used to justify the implementation of hazard areas according to FAA standards. These thresholds provide a reasonable understanding of the range and spread (distance deviated from nominal trajectory) of the vehicle and are a central focus of this current work. These zones would encompass the statistically probable flight paths upon exiting and reentering the NAS.

Analyzing the trajectory of the vehicle provides a STC that transitions from the NAS into the upper atmosphere and into space and back again. Mapping the transitional corridors would provide more accurate volumetric restrictions that conforms to the vehicle's flight trajectory - allowing for greater maneuverability and freedom of traversing aircraft. By opening up more potential flight paths in the regions around, significant reroutes in commercial flight planning becomes unnecessary; ultimately, avoiding increased flight times, fuel requirements, and seat costs.

Research was conducted using the Suborbital Space Flight Simulator (SSFS) at Embry-Riddle Aeronautical University's (ERAU) Applied Aviation Sciences (AAS) Department. The SSFS simulates suborbital flight of Virgin Galactic's SpaceShipTwo (SS2). This simulator runs X-Plane v.10 which is capable of recording over 56 flight parameters on a given mission. All data collected used for this present work was collected using the SSFS.

For each nominal flight, the SS2 was loaded with a takeoff mass of 12,587 kg - 1,020.1 kg for payload (including passengers), 4,535.9 kg dry mass, and 7,030.7 kg of fuel. This left a total of 5,556.3 kg remaining at landing [4]. After the vehicle is loaded, the mission may begin.

The nominal flight profile [5] begins with the SS2 vehicle dropping from WhiteKnighTwo at an altitude of 15.24

km (50,000 ft.). After a safe ignition distance is established (T+3 seconds) the engines are ignited. The ascent is established via a 2G pull to a +80° pitch angle. The powered ascent is continued until Main Engine Cutoff (MECO) at 45.72 km (150,000 ft.), after which SS2 operates as a glider for the remainder of the flight. The vehicle will continue through apogee and into the reentry phase of flight. It is during this time-frame within the upper stratosphere around the mesopause that most scientific experiments will be carried out. The limitations of X-Plane prevent the feathering mechanism of the flight vehicle to be accurately represented and is therefore not considered in this study. Upon completion of the reentry phase, the feathering mechanism will retract and the vehicle will begin a glide into landing. Thus concluding the nominal mission profile followed for this research.

## III. Flight Trajectories

Figure 1 shows the resultant flight trajectories of each flight flown on the X-Plane Simulation module for this study. Observing the patterns between the PoSSUM (red) and Control (black) flights, there seems to be no distinction between the two flight classifications. Each follow the strict flight pattern previously described with slight variations dependent on pilot with the PoSSUM flights undergoing slight correction maneuvers for scientific data collection. Even with these maneuvers, there seem to be no distinct visual separation between the two flight profiles.

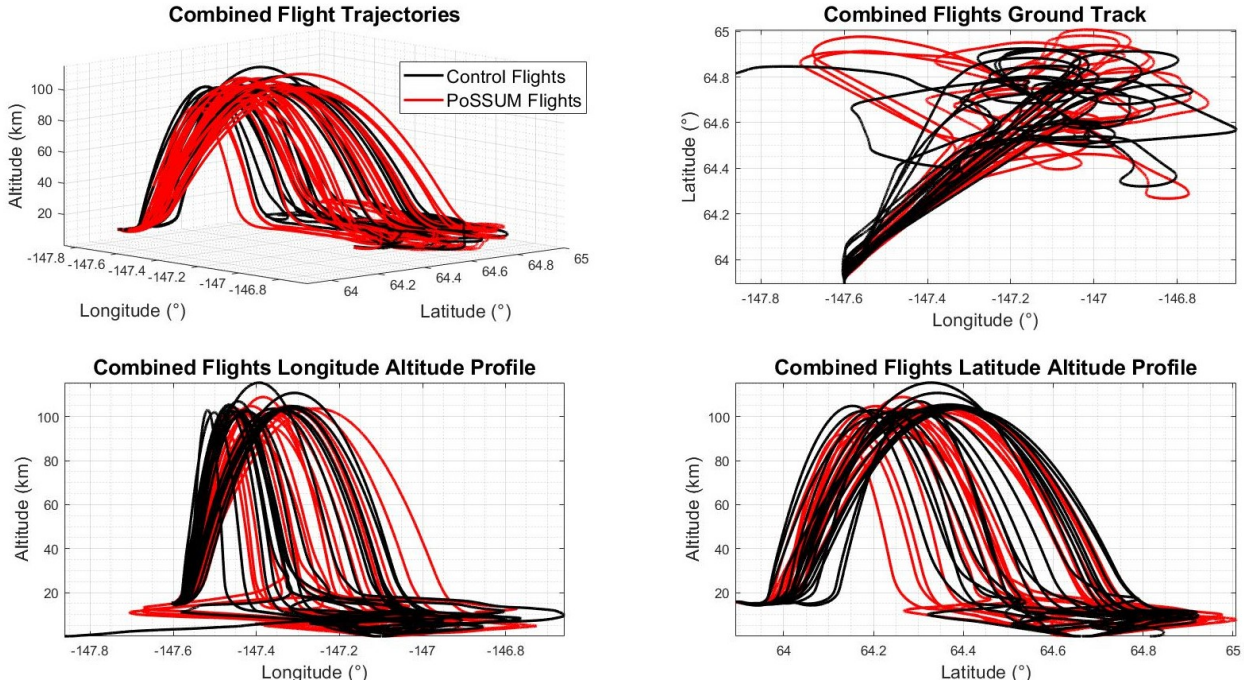


**Fig. 1 PoSSUM (red) and Control (black) full flight trajectories (top left) accompanied with ground track (top right), Longitude-Altitude (bottom left), and Latitude-Altitude (bottom right) profiles.**

While no distinction between the flight categories is clear, both seem to have wide variations in flight milestones, ascent Threshold (NAS Leave), Apogee, Descent Threshold (NAS Reentry), and glide flight patterns as will be discussed in Section V. Although these milestones occur in the same order and in a similar fashion for each flight category, the times and ranges at which these milestones occur can widely vary. Based on initial and visual observations, it would not be necessary for ATC and STM control to make significant changes to the incorporation of STC or compact envelopes based on a mission profile. This would prove helpful in further narrowing the required restricted airspace and safety criteria presented by the FAA.

Following the specified trajectory, Figure 2 displays the relationship of the altitude profile over the total elapsed mission time-of-flight, ToF, in relation to significant flight milestones - FL-600, Mesopause, and the Karman Line. Each

of these flight milestones represents a significant point along the flight's operational path and will be key in identifying deviations from the standard.

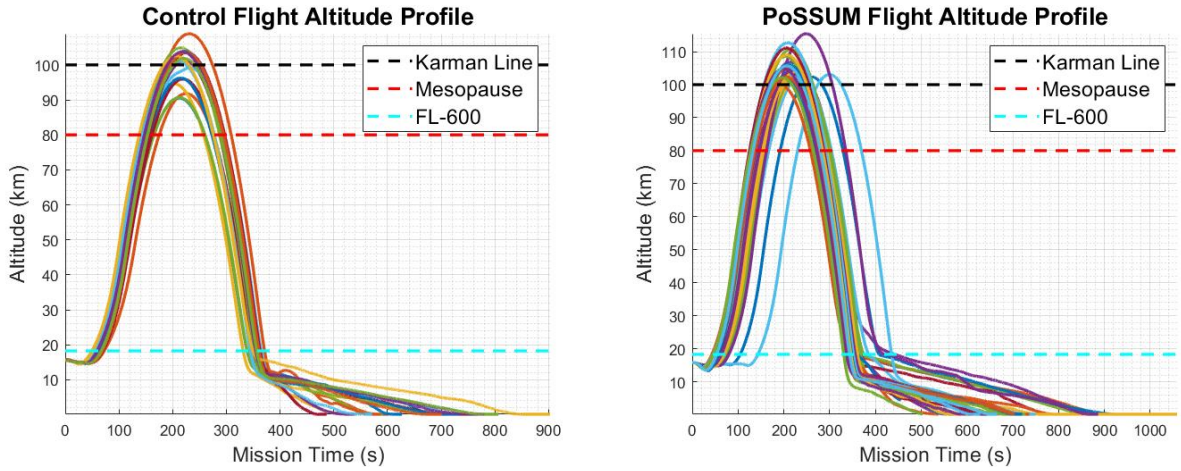


**(a) Control Flights** **(b) PoSSUM Flights**

**Fig. 2 Altitude time profiles - Control (left) and PoSSUM (right) - displayed in relation to significant flight milestones - FL-600, Mesopause, Karman Line.**

The differences in the mission flight parameters for each flight class resulted in 4.31 km difference in mean apogee height. Control flights had a mean of 100 ± 5.22 km and the PoSSUM flights had a mean of 104.3 ± 3.13 km. The difference in apogee altitudes is results from the different pilots used in for each flight class. The Control flights were flown by one pilot under ideal conditions, while the PoSSUM flights were flown by different pilots with control vector manipulations. Depending on the pilot's ability to fly the pre-determined ascent profile, apogee altitudes would differ. If the pilot's ascent angle was too shallow (below +75°), a lower apogee altitude would be achieved; and if the pilot's ascent angle was too steep (above +85°), a higher apogee altitude would be achieved.

The altitude differences affect the transition from reentry to glide as it changes the speed at which the vehicle levels for the glide phase. Higher apogees led to higher descent speeds, causing the pilot to have a more gradual transition to glide attitude to prevent excessive thermal and structural loadings on the vehicle.

Steeper ascent angles led to decreased lateral distances traveled, while shallower ascent angles increased lateral distance traveled. It is difficult for pilots to replicate exactly the same ascent angle from flight to flight and thus the ascent angle becomes a primary indicator of flight behavior.

## IV. Time Management

For these guided flights to be implemented effectively, a thorough understanding of these flight trajectories must be achieved. The integration of these unpowered, guided flight vehicles into the NAS is dependent on the temporal and spatial behavior inside of the NAS. While the vehicle remains above the NAS ceiling, it may be possible that air traffic may traverse underneath the flight path, time and hazard area permitting. Time is a large factor that affects the PoSSUM flight profiles, and will affect certain time dependent commercial operations.

The histograms displayed in Figure 3 show the average time the commercial space vehicle spent outside of the NAS to be 290.1 ± 8.3 seconds for Control flights and 300.5 ± 15.5 seconds for PoSSUM flights. Assuming a $3\sigma$ deviation safety standard, this leaves approximately 250 seconds for any potential traversing aircraft to pass underneath the flight path.

Under the current criteria presented by the FAA the safety area for the SS2 vehicle would extend 9.26 km (5 nmi) in the orthogonal direction to the space vehicle's velocity vector. Now, consider a commercial airliner traveling 900 km/hr (0.25 km/s) perpendicular to the flight path of the commercial space vehicle. This aircraft could travel the distance of the hazard area in approximately 37.0 seconds which leaves 213 seconds for safety margin. Note, this method assumes a

nominal trajectory without the possibility of catastrophic failure. The affect catastrophic space vehicle failure has on traversing aircraft pathways will be further investigated in a subsequent paper.

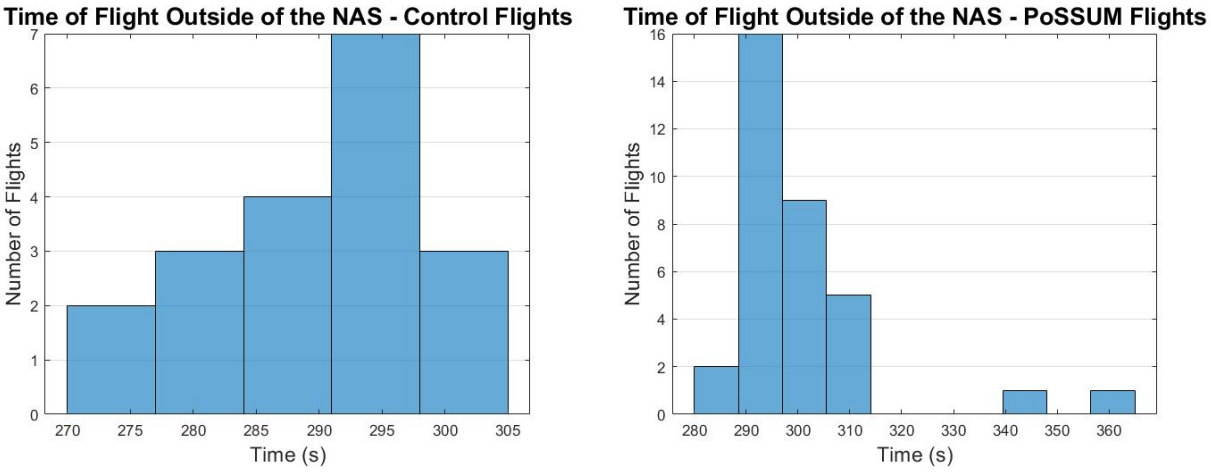


**(a) Control Flights** **(b) PoSSUM Flights**

**Fig. 3 Histogram displays of ToF outside of the NAS for Control (left) and PoSSUM (right) flights.**

While, on average the vehicle remains inside of the NAS for just over a minute upon ascent, much of the time spent inside of the NAS is during the descent portion of the trajectory or within the glide portion of the flight path. The best methods of integrating this portion of the flight into the NAS is still up for debate. The results presented are done so to describe the flight characteristics of the SS2 vehicle during its glide phase to provide reliable statistics to aid in the construction of integrating these flight paths in the NAS.

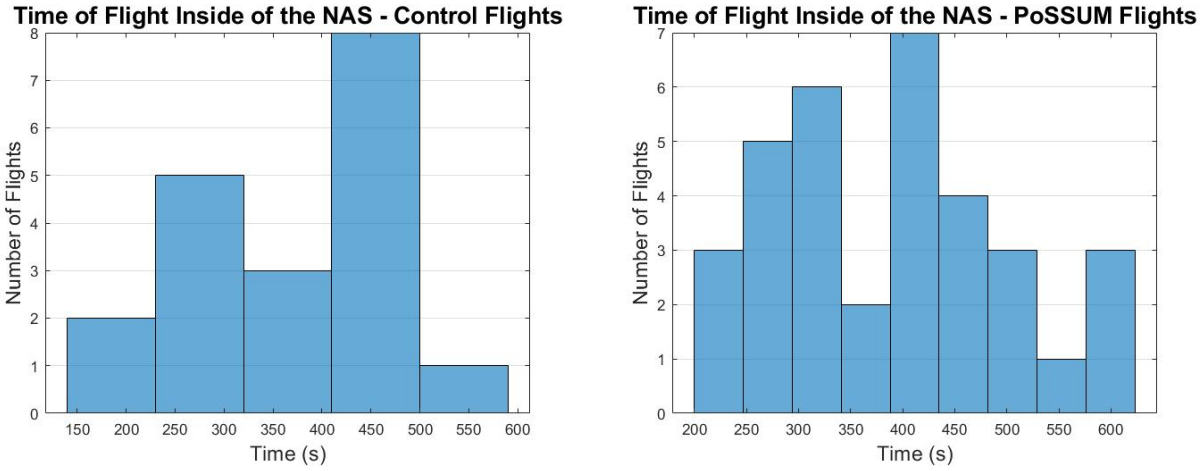


**(a) Control Flights** **(b) PoSSUM Flights**

**Fig. 4 Histogram displays of ToF inside of the NAS for Control (left) and PoSSUM (right) flights.**

Figure 4 displays a histogram of the total time the flight vehicle spent inside of FL-600 in both Control and PoSSUM flight scenarios. Initial results show PoSSUM flights spent 390.7 ± 112.4 seconds inside of the NAS, with 328.2 ±

106.9 seconds being within the descent trajectory of the vehicle. Unlike the ToF spent outside of the NAS, the ToF spent inside of the NAS was rather unpredictable and was highly reliant on the pilot determined path to the target landing area. The Control flights spent 366.1 ± 99.8 seconds inside of the NAS, 303.9 seconds of which were spent during the descent trajectory.

## V. Range Management

Discussed in the previous section are the characteristics of these SS2 flight trajectories in the temporal domain. This section will discuss the SS2 flight trajectories and their behavior in the spatial domain to thoroughly understand their performance for a comprehensive statistical analysis for effective commercial space vehicle integration.

### A. Ascent/Descent Thresholds

Two milestones that occur in any commercial space flight are the points at which it leaves and reenters the NAS at FL-600. Not only is this the point at which it crosses from ATC to STM control and vice versa, it serves as a significant indicator for potential hazard area positions and sizes. Understanding where these flights leave and reenter the NAS can be particulary informative of the flight's characteristics and allow for effective and efficient hazard areas to be implemented with little impact to the surrounding airspace and air traffic.

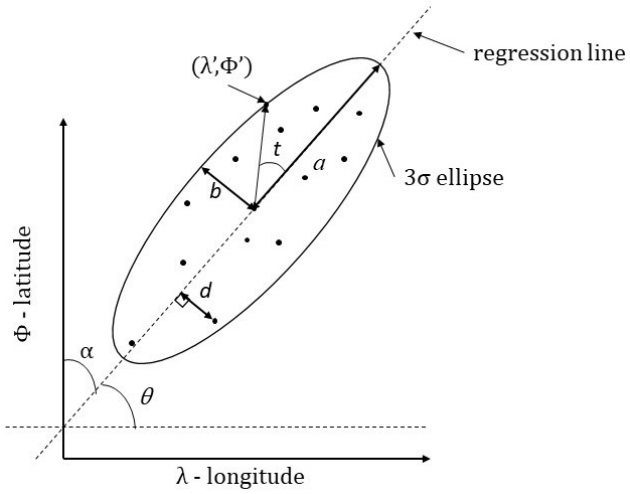


**Fig. 5 Ascent/Descent Threshold Oval diagram depicting key parameters for threshold construction.**

Establishing the ascent/descent thresholds began with the assumption that the least squares approximation of the data points was the idealistic nominal flight path.

$$\phi = \frac{\Delta\phi}{\Delta\lambda}\lambda + s \tag{1}$$

Equation 1 displays the relationship between flight latitude and longitude in the form of a linear regression where $\phi$ is the latitude, $\Delta\phi$ is the linear change in latitude, $\lambda$ is the longitude, $\Delta\lambda$ is the linear change in longitude, and $s$ is the constant determined from the linear regression approximation, as the latitude (y) - intercept.

The placement of these ascent and descent thresholds is dependent on the flight range and flight azimuth, while the size is dependent on the standard deviations of the range and a quantifiable metric for the cross-range spread, $d$, shown in Figure 6. Depicted is a generalization of determining the orthogonal distance from a specified point to a line. The line:

$$y = mx + b \tag{2}$$

is representative of the linear regression line shown in Equation 1, an additional parallel line is drawn through the point of interest shown as:

$$y - k = m(x - z) \tag{3}$$

For computational ease, a perpendicular line:

$$y = -\frac{1}{m}x \tag{4}$$

was drawn through the origin. The intersections of Equation 4 and Equations 2 and 3 were used as $x_0$, $y_0$, $x_1$, and $y_1$ in the distance equation depicted in Equation 5:

$$d = \sqrt{(x_0 - x_1)^2 + (y_0 - y_1)^2} \tag{5}$$

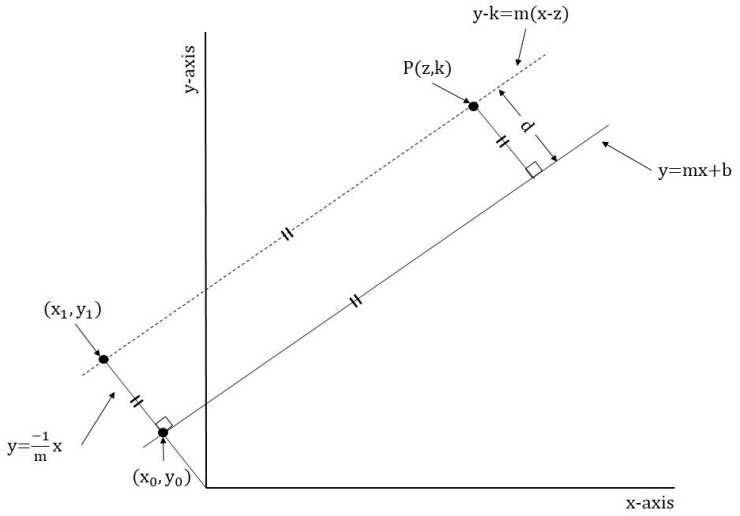


**Fig. 6 Depiction of the generalization of the threshold construction problem used to calculate the distance from each NAS entry/reentry points to the linear regression line used as the standard.**

Setting Equation 4 equal to Equation 2 and solving for $x$, we define $x_1$ to be the $x$ intersecting coordinate of the perpendicular line and the linear regression line:

$$x_1 = \frac{b}{-m - \frac{1}{m}} \tag{6}$$

Plugging Equation 6 back into Equation 4 the corresponding $y$ coordinate is found in $y_1$:

$$y_1 = \frac{b}{m^2 + 1} \tag{7}$$

Now, setting Equation 4 equal to Equation 3 and solving for $x$, $x_0$ is obtained and is the $x$ intersection of the perpendicular line and the line containing the point of interest:

$$x_0 = \frac{k - mz}{-m - \frac{1}{m}} \tag{8}$$

Plugging Equation 8 back into Equation 4 the corresponding $y$ coordinate is found in $y_0$:

$$y_1 = \frac{k - mz}{m^2 + 1} \tag{9}$$

Inserting these values found in Equations 6, 7, 8, 9 into the distance equation, Equation 5, we get the distance from the regression line to line containing the point of interest in terms of the intersection points:

$$d = \sqrt{\left(\frac{b + mz - k}{m + \frac{1}{m}}\right)^2 + \left(\frac{-b - mz + k}{m^2 + 1}\right)^2} \tag{10}$$

Multiplying the first term by $\frac{m^2}{m^2}$ Equation 10 becomes:

$$d = \sqrt{\left(\frac{mb + m^2 z - mk}{m^2 + 1}\right)^2 + \left(\frac{-b - mz + k}{m^2 + 1}\right)^2} \tag{11}$$

Factoring the $m^2 + 1$ in the denominator and $-m$ in the numerator of the first term Equation 11 becomes:

$$d = \frac{\sqrt{[-m(k - mz - b)]^2 + (k - mz - b)^2}}{m^2 + 1} \tag{12}$$

The $k - mz - b$ term may be pulled out, and because $(-m)^2 = m^2$ Equation 12 rewrites to:

$$d = \frac{|k - mz - b|}{\sqrt{(m)^2 + 1}} \tag{13}$$

Putting Equation 13 in terms of the relevant variables for the threshold problem yields:

$$d = \frac{|\phi - \frac{\Delta\phi}{\Delta\lambda}(\lambda) - s|}{\sqrt{\left(\frac{\Delta\phi}{\Delta\lambda}\right)^2 + 1}} \tag{14}$$

where $m \equiv \frac{\Delta\phi}{\Delta\lambda}$. This method was chosen over the better know distance equation:

$$d = \frac{|Ax_0 + By_0 + C|}{\sqrt{A^2 + B^2}}$$

because $m \equiv \frac{\Delta\phi}{\Delta\lambda}$ is a directly calculable value from a given flight azimuth, and $A$, $B$, and $C$ are not directly calculable from the available flight data and require $\Delta\phi$ and $\Delta\lambda$ to be separated. The drawn ovals in Figure 7 are representative of the $3\sigma$ down-range (semi-major axis, a) and cross-range distances (semi-minor axis, b):

$$\begin{aligned} a &= 3\sigma_{range} \\ b &= 3\sigma_d \end{aligned} \tag{15}$$

The threshold ovals were drawn at $3\sigma$ deviations from the mean latitude and longitude threshold for both ascent and descent trajectories.

Now that the size of these thresholds have been defined, a method of determining the orientation of these thresholds is explored. To begin, a relationship between the angle $\theta$ and the given $m$ value in the linear regression equation. Knowing $m \equiv \frac{\Delta\phi}{\Delta\lambda}$, it may be said that:

$$\theta = \operatorname{arccot}\left(\frac{\Delta\phi}{\Delta\lambda}\right) \tag{16}$$

where $\theta$ is the rotation angle between the linear regression line and the horizontal as shown in Figure 5. For any non-rotated ellipse centered on the origin:

$$\begin{bmatrix} \lambda_1 \\ \phi_1 \end{bmatrix} = \begin{bmatrix} \cos t & 0 \\ 0 & \sin t \end{bmatrix} \begin{bmatrix} a \\ b \end{bmatrix} \tag{17}$$

while a rotated ellipse is described by Equation 18:

$$\begin{bmatrix} \lambda \\ \phi \end{bmatrix} = \begin{bmatrix} \cos\theta & -\sin\theta \\ \sin\theta & \cos\theta \end{bmatrix} \begin{bmatrix} \lambda_1 \\ \phi_1 \end{bmatrix} \tag{18}$$

Combining Equations 17 and 18 and incorporating the mean latitude and longitude translations yields Equation 19 and represents the ascent and descent thresholds [6]:

$$\begin{bmatrix} \lambda' \\ \phi' \end{bmatrix} = \begin{bmatrix} \cos t \cos\theta & -\sin t \sin\theta \\ \cos t \sin\theta & \sin t \cos\theta \end{bmatrix} \begin{bmatrix} a \\ b \end{bmatrix} + \begin{bmatrix} \overline{\lambda} \\ \overline{\phi} \end{bmatrix} \tag{19}$$

where $\overline{\lambda}$ and $\overline{\phi}$ are the mean longitude and latitude of the flight data set, t is the parameterized variable from 0 to $2\pi$ beginning on the linear regression line, and $\lambda'$ and $\phi'$ are the respective longitude and latitude values associated with angle $t$ and draw out the threshold border (see Figure 5).

The map displayed in Figure 7 presents the coordinates at which the SS2 vehicle ascends out of an descends into the NAS with the safety oval generated from a $3\sigma$ deviation from the sample average longitude and latitude. The total footprint of these flight patterns covers no more than a $1^\circ \times 1^\circ$ section of airspace, and restrictions larger than this will be extraneous and unnecessary for flight hazard areas. Further study will be required to incorporate additional flight parameters to further tailor these STCs to fit the pre-determined flight trajectory.

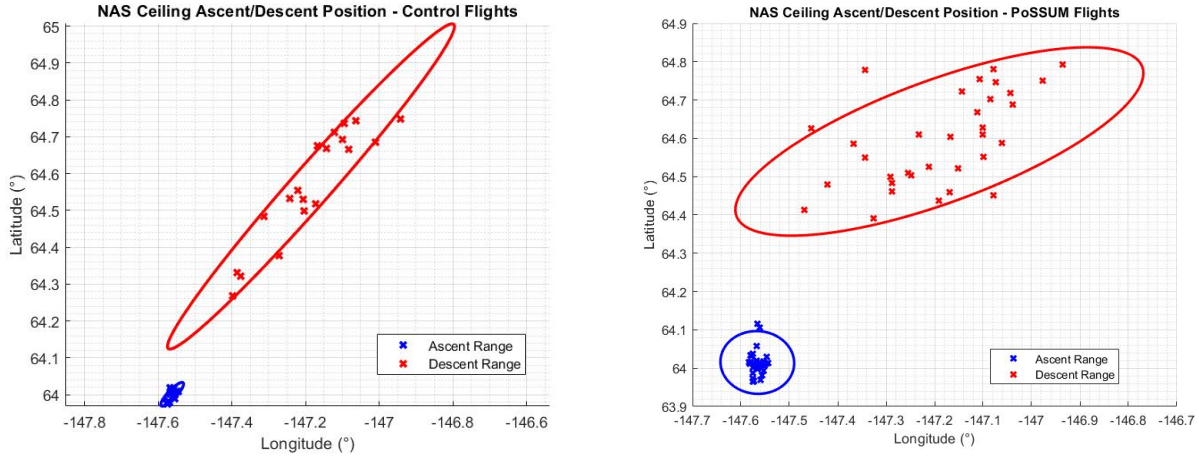


**(a) Control Flights** **(b) PoSSUM Flights**

**Fig. 7 Latitude-Longitude map of FL-600 ascent and descent thresholds. Ascent (blue) and descent (orange) points are displayed for both Control (left) and PoSSUM (right) flights encircled by a $3\sigma$ deviation in the down-range and cross-range directions.**

The numerical data displayed in Table 1 is directly calculated using the methodology described above from the data obtained during PoSSUM and Control flight campaigns. Overall, the PoSSUM flight parameters differed greatly compared to their Control flight counterparts. In exception to the mean latitude and longitude, all parameters differed by greater than 30%. The data suggests a large dispersion as a result of the scientific data collection maneuvers, with little effect on the mean flight pattern of the vehicle. A noticeable change is seen in the change in flight azimuth from ascent to descent trajectories within the PoSSUM flight category. With an approximately 2° change in flight azimuth, the Control flights maintained a relatively straight flight pattern when compared to their PoSSUM counterparts, which had a 17.5° change in flight azimuth from the ascent to descent thresholds.

It is important to understand the characteristics of these flights collectively and to know their differences to appropriately characterize them so effective no-fly zones, and hazard areas may be implemented. The ascent threshold is important for a brief portion of the flights as the vehicle drops from the launch vehicle, accelerates, and pitches up to begin the mission.

While the exact coordinates of the ascent and descent thresholds are not significant, the down-range and cross-range spread over which they occur provide critical information to how these flights may be implemented into the NAS [7]. Visually, as observed in Figure 7, the PoSSUM flights yielded a 146.6% spread for ascent and a 97.18% spread for the descent thresholds. The spread observed from the PoSSUM flights is due to mission constraints, parameters, and flight

**Table 1 Parametric study of both flight data sets for descent (Table 1a) and ascent (Table 1b) trajectories. The thresholds shown in Figure 7 were constructed using the values presented.**

**(a) Descent Parameters**

| Control | | PoSSUM | | Percent Diff. |
|---|---|---|---|---|
| $a_c$ | 65.18km | $a_p$ | 47.45km | 31.48% |
| $b_c$ | 5.93km | $b_p$ | 17.14km | 97.18% |
| $\alpha_c$ | 48.62° | $\alpha_p$ | 26.04° | 60.49% |
| $\theta_c$ | 41.38° | $\theta_p$ | 63.96° | 42.87% |
| $\overline{\lambda}_c$ | -147.185° | $\overline{\lambda}_p$ | -147.566° | 0.259% |
| $\overline{\phi}_c$ | 64.565° | $\overline{\phi}_p$ | 64.015° | 0.856% |

**(b) Ascent Parameters**

| Control | | PoSSUM | | Percent Diff. |
|---|---|---|---|---|
| $a_c$ | 4.79km | $a_p$ | 9.12km | 62.26% |
| $b_c$ | 1.30km | $b_p$ | 8.44km | 146.6% |
| $\alpha_c$ | 46.471° | $\alpha_p$ | 8.511° | 138.1% |
| $\theta_c$ | 43.53° | $\theta_p$ | 81.49° | 60.73% |
| $\overline{\lambda}_c$ | -147.562° | $\overline{\lambda}_p$ | -147.190° | 0.252% |
| $\overline{\phi}_c$ | 64.001° | $\overline{\phi}_p$ | 64.592° | 0.919% |

styles of the operators. Flights from Project PoSSUM followed a general flight profile to meet mission requirements such as altitude and time in the mesosphere, but the flights were not required to adhere to a specific profile. The pilots were the largest factor in the range of exit and entry points of the NAS. Due to the scheduling of PoSSUM, different pilots were operating the simulator to conduct flights. The difference in the skill levels, thought, judgement, and overall flight styles caused changes in the range of ascent thresholds. However, during the descent phase, this spread was primarily attributed to the data collection processes that occurred within the stratosphere. This spread was quantified by applying linear regression techniques and calculating the correlation coefficient of the longitude to latitude relationship. The Control flights were much tighter, R=0.62 (ascent) and R=0.93 (descent), than the PoSSUM counterparts, R=0.43 (ascent) and R=0.54 (descent). The high correlation observed in the Control flights leads to greater reliability and accuracy when predicting the exact coordinates of the descent threshold and shows the PoSSUM flights were susceptible to the scientific data collection processes that occurred.

### B. Range Limits

While the data collection processes present in the PoSSUM flights affected the spread of the descent threshold position, the descent threshold range was not as sensitive to the scientific operations. This is evident in Figure 8 where the descent threshold for control flights are at a range of 80.6 ± 6.5 km and 71.3 ± 7.3 km for PoSSUM flights.

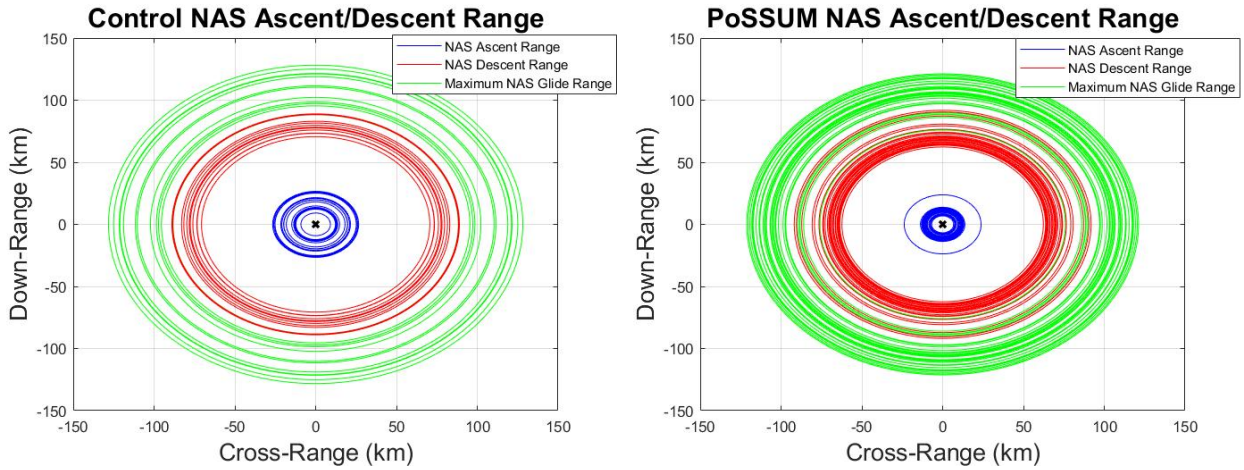


**(a) Control Flights** **(b) PoSSUM Flights**

**Fig. 8 Cross-range and down-range map displaying ascent range (blue), and descent range (red), and maximum glide range (green) observed over the sample flights.**

Where the ascent threshold ranges are 17.9 ± 5.8 km and 10.7 ± 3.1 km for control and PoSSUM flights respectively. The ranges presented are calculated based on a projection of the flight path onto the X-Y plane looking down the Z-axis.

This provides a more accurate representation of where the vehicle will cross the NAS ceiling and reach its maximum lateral distance from drop. The disparity between the ascent and descent threshold of just over 60 km remains open for in between 200-300 seconds, according to Figure 3, which may be used for air traffic pathways. This disparity is observed as a large white gap in Figure 8 between the blue ascent range indicators, and the red descent range indicators. Further investigation will be necessary to determine to the potential of using this strip of airspace as emergency air traffic routes to take into account CSV flight contingency scenarios.

The maximum glide range presented by both flight profiles are near indistinguishable. With the maximum range for Control flights being 103.8 ± 15.1 km and the maximum for PoSSUM flights being 104.7 ± 12.4 km. While the flight vehicles maintain the capability to exceed the maximum range, it must be noted for nominal scenarios, the remains little reason for these vehicles to exceed the glide ranges displayed. Pre-chosen launch and landing sites play a critical role in the maximum glide range which are significantly effected by flight maneuvers used to setup the landing procedure. These maneuvers include but are not limited to velocity dissipation, scientific data collection, and approach heading adjustments.

### C. Debris Dispersion

One of the objectives of this preliminary study was to have a better understanding of the debris footprint size and evolutions during the ascent and descent segments of a suborbital trajectory. A provisional hazard area model [8] can be used as a first order approximation for out analysis as displayed by the equations below:

$$\text{Debris Area Length (km)} \approx \frac{Alt(feet)}{1000}$$

$$\text{Debris Area Width (km)} \approx \frac{DebrisAreaLength}{8}$$

These equations were derived from the Columbia accident (explosion at about 230,000 feet with debris area length of about 400 km and debris area width of about 65 km) measurements and they are only valid for vehicles with similar trajectory behaviors. Another debris area model could be used from the measurements of SpaceShipTwo accident in 2014. After the vehicle broke apart at about 50,000 feet, it created a 56 km long debris field area. Note: 50,000 feet/56 km ≈ 900, which is a similar factor as the Columbia case as shown in the previous equation. We can assume the debris area width for the SpaceShipTwo case is about 8 km:

$$\text{Debris Area Length (km)} \approx \frac{Alt(feet)}{900}$$

$$\text{Debris Area Width (km)} \approx \frac{DebrisAreaLength}{7}$$

In our analysis, the suborbital flights were flown in the vicinity of the Daytona Beach International Airport in Daytona Beach as simulated with the SSFS. This means that all trajectories have a northern launch azimuth of 90° (East) and the debris impact footprints during ascent and descent will occur over the Atlantic Ocean. Since all trajectories have different pitch angles (around 80°-85°), the debris area parameters (length and width) will vary. In addition, since possible hazards (explosions and breakups, engine shutdown failure, malfunction turns, etc.) could be associated [9, 10] during the ascent and descent portions of the suborbital trajectory the debris area will also be affected.

## VI. Conclusions and Future Work

Visually, the sample flight trajectories from the PoSSUM and Control campaigns exhibit similar behavior over the entirety of the flight pattern. From air-takeoff to the glide phase, each follow a parabolic trajectory that may or may not be expanded in the velocity vector direction, and during the glide phase to landing each exhibit flight patterns dominated by pilot discretion. Apogee for both PoSSUM and Control flight campaigns crossed the Karman Line, and into space, yet a 4 km difference remained in the mean apogee altitude. This difference is not indicative of differences in flight patterns between the campaigns rather is due to vehicular instability around the nominal ascent pitch angles.

The flight characteristics of these flights within the temporal domain were also studied with special attention to ToF inside and out of the NAS. Mean ToF outside NAS remained between 290-300 seconds for each flight campaign, while mean ToF inside the NAS was between 365-390 seconds but varied much more widely due to the reliance on pilot

discretion. A potential for air traffic routes while the CSV remains outside the NAS was also noted pending further study of CSV debris dispersion .

A primary focus of this paper was placed in the spatial domain to determine where key flight milestones occurred, in particular, in relation to FL-600. The results gathered show a disparity in the cross-range spread of the PoSSUM flights when compared to their Control counterparts, a 97.18% difference in the descent threshold. This disparity, alongside the 17.5° change in flight azimuth, show a dependence on the flight maneuvers introduced during the PoSSUM campaigns. However, no change in the mean latitude and longitude is observed, all percent differences are maintained under 0.1%. It was also noted that the entirety of the flight trajectories remains within a $1^\circ \times 1^\circ$ section of the airspace. Any flight restrictions larger than this $1^\circ \times 1^\circ$ airspace will cause unnecessary interruptions to air traffic patterns. However, this study does not take into account contingency scenarios or debris dispersion analysis. The incorporation of these parameters may increase the footprint of these flight trajectories, yet the $1^\circ \times 1^\circ$ footprint provides a baseline from which to make initial judgments regarding airspace closures onto which contingency scenarios may be appended.

A parametric method of drawing ascent and descent NAS thresholds was presented to aid mission planners in understanding all possible nominal outcomes for guided CSV flights, and how these flights may interface between the STM and ATC. This method puts a significant focus on statistically determining the most probable NAS exit and entry locations so appropriate STCs and air traffic routes may be constructed.

As future campaigns will be flown in the SSFS the flight data pool will continue to increase and allow for more precise predictions these CSV flights will have on the current air traffic network. While these flights will change the data present, it is not expected that these upcoming flights will change the data by significant margins. Future work will analyze these trajectories as functions of space and time to statistically compute spatial and temporal parameters of proposed STCs and air traffic routes in the STC vicinity. Additional research will explore STC optimization for minimal air traffic interruption, and controllability of STCs during nominal and contingency scenarios. Debris dispersion analysis will be incorporated in addition to nominal scenarios to construct full STCs to FAA safety standards.

## Acknowledgements

The authors would like to acknowledge the Applied Aviation Sciences Department at Embry-Riddle Aeronautical University for supporting this research. The authors would also like to recognize the SSFS pilots - Chris Nguyen and Eugenie Fontaine - for their efforts and contributions to the data collection process of producing this work.

## References

[1] Colvin, T. J., and Alonso, J. J., "Compact envelopes and SU-FARM for integrated air-and-space traffic management," *53rd AIAA Aerospace Sciences Meeting*, 2015, p. 1822.

[2] Tinoco, J. K., Firmo, R., Yu, C., Moallemi, M., Castro, C., and Waller, T., "Commercial Space Transportation: A Simulation and Analysis of Operations Impacts on the United States National Airspace System and Airline Stakeholders," 2018.

[3] Cheng, V., Diaz, G., and Sridhar, B., "Flight Safety Analysis Tool for Space Vehicle Operations in the National Airspace," *AIAA's 3rd Annual Aviation Technology, Integration, and Operations (ATIO) Forum*, 2003, p. 6793.

[4] Deng, A., "The Prediction of Aerodynamic Performance and Handling Quality of SpaceShipTwo Based on the Analysis of SpaceShipOne Flight Test Data," 2012.

[5] Llanos, P. J., and Hays, C., "Flight Operations Quality Assurance Analysis for Contingency Scenarios of SpaceShipTwo using ERAU's Suborbital Space Flight Simulator," *AIAA SPACE and Astronautics Forum and Exposition*, 2017, p. 5111.

[6] Hendricks, M. C., "Rotated Ellipses and Their Intersections with Lines," 2012.

[7] Llanos, P., Seedhouse, E., and Hays, C., "Nominal SpaceShipTwo Flights conducted by Scientist-Astronaut Candidates in a Suborbital Space Flight Simulator," 2018.

[8] Morlang, F., Ferrand, J., and Seker, R., "Why a future commercial spacecraft must be able to SWIM," *Journal of Space Safety Engineering*, Vol. 4, No. 1, 2017, pp. 5–8.

[9] Sarconi, M., "A Prototype System for Simulating the Risks of Sub-Orbital Space Flight for Commercial Aviation," , 2013.

[10] Torio, A. M., Bahu, J., Delorme, D., Guenard, V., and Poussin, H., "Near range safety analysis for a reusable launcher concept based on toss-back," *Journal of space safety engineering*, Vol. 4, No. 1, 2017, pp. 29–35.